Earth and Planetary Science Letters 364 (2013) 44–58

Contents lists available at SciVerse ScienceDirect

Earth and Planetary Science Letters

journal homepage: www.elsevier.com/locate/epsl

Extension of continental crust by anelastic deformation during the 2011 Tohoku-oki earthquake: The role of extensional faulting in the generation of a great tsunami

Takeshi Tsuji [a,*], Kiichiro Kawamura [b], Toshiya Kanamatsu [c], Takafumi Kasaya [c], Katsunori Fujikura [c], Yoshihiro Ito [d], Tetsuro Tsuru [e], Masataka Kinoshita [c]

[a] International Institute for Carbon-Neutral Energy Research (WPI-I2CNER), Kyushu University, 744 Motooka, Nishi-ku, Fukuoka 819-0395, Japan
[b] Faculty of Science, Yamaguchi University, Yamaguchi, Japan
[c] Japan Agency for Marine–Earth Science and Technology, Yokosuka, Japan
[d] Graduate School of Science, Tohoku University, Miyagi, Japan
[e] COSMO Oil Co. Ltd., Tokyo, Japan

ARTICLE INFO

Article history:
Received 20 September 2012
Received in revised form
27 December 2012
Accepted 29 December 2012
Editor: P. Shearer

Keywords:
2011 Tohoku-oki earthquake
tsunami mechanisms
seafloor observations
normal fault
anelastic deformation
heat flow

ABSTRACT

Observations of seafloor morphologies and environments made before and after the 2011 Tohoku-oki earthquake reveal open fissures, generated during the earthquake, where the fault trace is interpreted on seismic profiles to intersect the seafloor. Anomalously high heat flow was observed at a landward-dipping normal fault in August 2011, five months after the earthquake, but by August 2012 heat flow measured at the same station had decreased to close to the background value, which suggests that the normal fault ruptured during the 2011 earthquake. These seafloor observations and measurements demonstrate deformation that was both extensional and anelastic within the overriding continental plate during the 2011 earthquake. Seismic profiles as well as seafloor bathymetry data in the tsunami source area further demonstrate that landward-dipping normal faults (extensional faults) collapse the continental framework and detach the seaward frontal crust from the landward crust at far landward from the trench. The extensional and anelastic deformation (i.e., normal faulting) observed in both seafloor observations and seismic profiles allows the smooth seaward movement of the continental crust. Seaward extension of the continental crust close to the trench axis in response to normal faulting is a characteristic structure of tsunami source areas, as similar landward-dipping normal faults have been observed at other convergent plate margins where tsunamigenic earthquakes have occurred. We propose that the existence of a normal fault that moves the continental crust close to the trench can be considered one indicator of a source area for a huge tsunami.

1. Introduction

Interplate earthquakes and tsunamis are frequently generated in the Japan Trench (Yamanaka and Kikuchi, 2004), where the Pacific plate is subducting beneath the Japan Arc at the high convergence rate of 8.6 cm/yr (DeMets et al., 1990). The rupture areas of many interplate earthquakes recorded before the 2011 Tohoku-oki earthquake in this convergent plate margin were limited to small rupture segments. However, the 2011 Tohoku-oki earthquake (Mw 9.0) ruptured a wide area along the plate interface (~450 km in the trench-parallel direction; Ide et al., 2011) and generated a particularly large tsunami (Fujii et al., 2011; Maeda et al., 2011). On the basis of geodetic and geophysical data as well as tsunami records, large slip along the plate interface (~60 m) was estimated to have occurred near the trench off Miyagi (Fig. 1; Maeda et al., 2011; Ito et al., 2011; Sato et al., 2011; Kido et al., 2011; Fujiwara et al., 2011; Lay et al., 2011). The region where the rupture propagated to the trench corresponds to the generation area of the huge tsunami (Fujii et al., 2011; Maeda et al., 2011). Therefore, large plate-boundary slip near the trench seems to have been a primary mechanism of tsunami generation in the 2011 earthquake, although seafloor slumping must also be considered as one of the tsunami-generating mechanisms (e.g., Kawamura et al., 2012; Grilli et al., 2012). In other subduction zones, coseismic slip propagating to near the trench is also thought to contribute to tsunami generation (Kanamori and Kikuchi, 1993; Henstock et al., 2006; Gulick

* Corresponding author. Tel./fax: +81 92 802 6875.
E-mail addresses: tsuji@i2cner.kyushu-u.ac.jp (T. Tsuji), kiichiro@sci.yamaguchi-u.ac.jp (K. Kawamura), toshiyak@jamstec.go.jp (T. Kanamatsu), tkasa@jamstec.go.jp (T. Kasaya), fujikura@jamstec.go.jp (K. Fujikura), yito@aob.gp.tohoku.ac.jp (Y. Ito), tetsuro_tsuru@cosmo-oil.co.jp (T. Tsuru), masa@jamstec.go.jp (M. Kinoshita).

0012-821X/$ - see front matter © 2013 Elsevier B.V. All rights reserved.
http://dx.doi.org/10.1016/j.epsl.2012.12.038

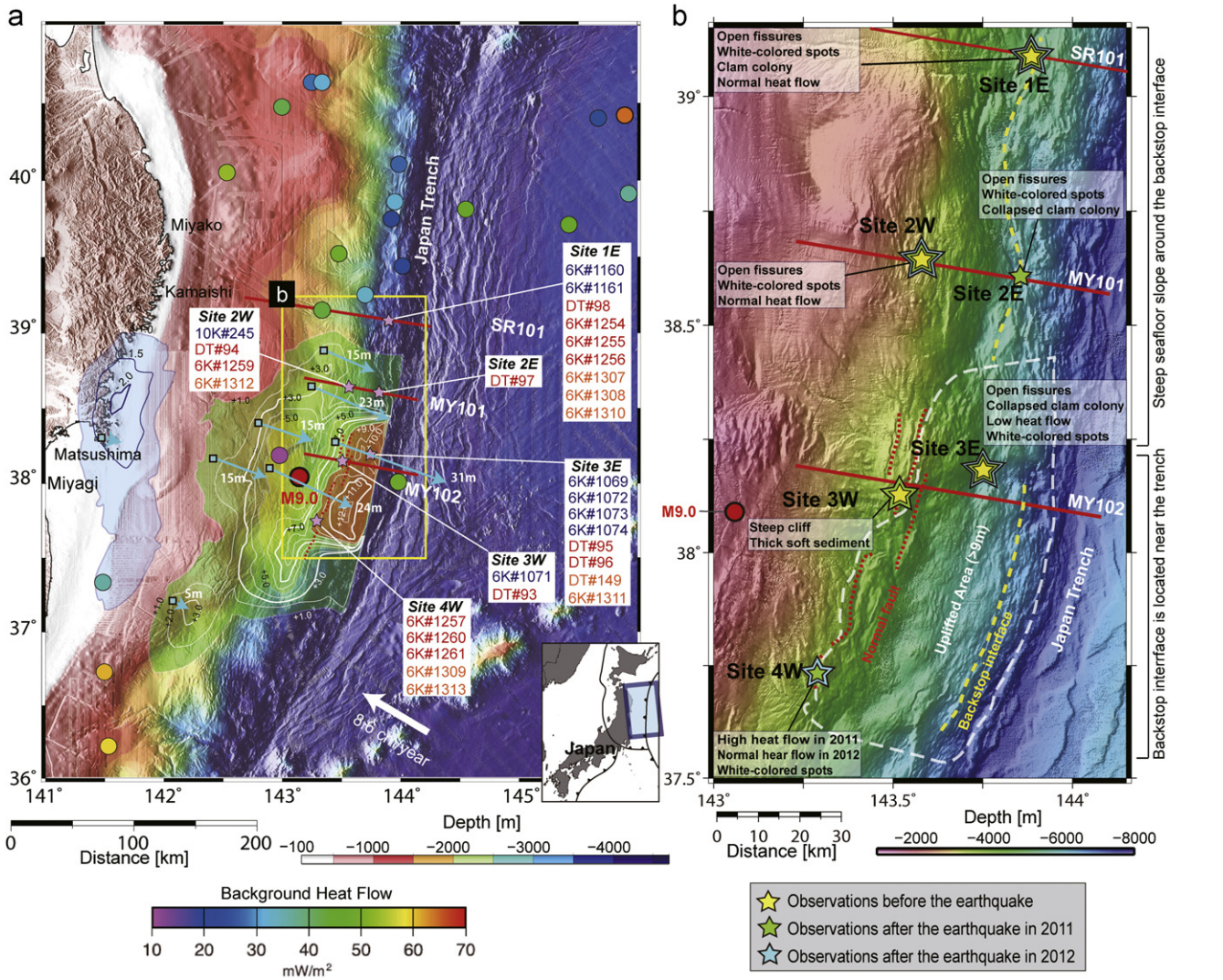

Fig. 1. Index maps for the 2011 Tohoku-oki earthquake in the Japan Trench (JCG, JAMSTEC, 2011). (a) Blue and white contour lines are subsidence and uplift, respectively, estimated from tsunami inversion (Fujii et al., 2011), with contour intervals of 0.5 m (subsidence) and 1.0 m (uplift). Blue arrows indicate dynamic seafloor displacements observed at seafloor observatories (Kido et al., 2011; Sato et al., 2011). Red lines are locations of seismic profiles (SR101, MY101, and MY102) shown in Fig. 2. Stars indicate diving sites and are labeled with dive numbers of pre-earthquake observations (blue numerals) and post-earthquake observations in 2011 (red numerals) and in 2012 (orange numerals). Background heat flow values measured before the 2011 earthquake are displayed as colored dots (Yamano et al., 2008; Kimura et al., 2012). (b) Enlarged map around the diving sites, corresponding to the yellow rectangle in panel (a). Red dashed lines indicate seafloor traces of normal faults (i.e., ridge structures). Yellow dashed lines indicate estimated locations of the backstop interface. The white dashed line indicates the boundary of the area of significant seafloor uplift (>9 m uplift) and also the tsunami generation area (Fujii et al., 2011), corresponding to the reddish-brown area in panel (a). Observations made during the post-earthquake dives are described in panel (b).

et al., 2011). Seismological studies (e.g., Koper et al., 2011) have demonstrated that large slip along the shallow plate interface near the trench is a characteristic of tsunamigenic earthquakes that produce anomalously large tsunamis relative to the seismic energy (Kanamori, 1972). However, the mechanisms of large displacement along the plate interface near the trench are not well understood. Prior to the 2011 Tohoku-oki earthquake, the plate interface near the Japan Trench was thought to be too weak to accumulate strain and, because of this presumed weak lithology, the frontal prism was expected to deform aseismically (Kerr, 2011).

As a mechanism of the large coseismic displacement near the trench during the 2011 earthquake, McKenzie and Jackson (2012) demonstrated that the release of gravitational potential energy can induce a pop-up movement of the frontal prism. Because tectonic erosion has generated a steep seafloor slope ($\sim 8^{\circ}$) near the trench (Von Huene et al., 2004), the wedge is gravitationally unstable, and gravitational potential energy could thus easily have been released during the earthquake (McKenzie and Jackson, 2012; Kawamura et al., 2012). Indeed, seafloor slumping due to gravitational instability that occurred during the 2011 earthquake has been clearly observed at the trench axis (Fujiwara et al., 2011; Kodaira et al., 2012). Pore pressure increasing due to clay dehydration is further proposed for low shear strength along the plate interface allowing runaway slip to the trench (Kimura et al., 2012).

On the basis of seismic profile acquired at the tsunami source area, Tsuji et al. (2011) proposed that large displacement along the plate interface near the trench generated a tensile state of stress within the geological units above the plate interface, resulting in rupture along normal faults. Such normal faulting is common at erosional margins such as the Tohoku margin (e.g., Von Huene et al., 2004). During the 2011 earthquake, normal faulting aftershocks generated in the overriding plate (Asano

et al., 2011) are evidence of extensional activity there. Furthermore, geodetic data (Ito et al., 2011; Kido et al., 2011) also indicate that significant extension was generated coseismically within the overriding plate close to the trench. Therefore, the geological structures and dynamic activity within the overriding plate are important for understanding both the mechanisms of large displacements along the plate interface and the mechanisms of tsunami generation.

In this paper, we identify a series of faults in seismic reflection profiles acquired within and outside of the tsunami source area and examine dynamic changes of the fault traces on the seafloor by comparing observations made during submersible dives before and after the 2011 earthquake, in order to identify characteristic geological structures and dynamic fault activity within the overriding plate in the tsunami source area. During the seafloor observations, we also repeatedly measured heat flow to evaluate the activity of the fault system. These are the first time-lapse observations of the seafloor and the first heat flow measurements made in the tsunami generation area of the 2011 earthquake. Because our survey area includes the region of largest vertical displacement in the vicinity of the source region of the Tohoku-oki earthquake (Fig. 1) (Fujii et al., 2011; Hayashi et al., 2011; Tsuji et al., 2011; Ito et al., 2011), these shallow faults are most likely related to the tsunami generation mechanism. Because the long-period slip near the trench that resulted in the huge tsunami generated almost no seismic energy (Koper et al., 2011), the tsunamigenic rupture process near the trench cannot be clearly determined by using only onshore seismometer data. However, direct observations and measurements of the seafloor fault traces identified on seismic reflection profiles can potentially provide direct evidence of the generation mechanism of the huge tsunami. Further, we compare the geological structures in the Japan Trench with those of other convergent plate margins and discuss the global implications of our proposed rupture mechanisms leading to tsunami generation.

2. Methods

2.1. Seismic reflection data

The geologic structure in the vicinity of the most strongly uplifted area in the source region of the 2011 Tohoku-oki earthquake (Fig. 1) was inferred from seismic data collected prior to the event. Multi-channel seismic reflection data were acquired by the R/V *Kairei* (Japan Agency for Marine-Earth Science and Technology) in 1997 (cruise KR97-07) and 1999 (cruise KR99-08) (Tsuru et al., 2002). Both of these seismic surveys used a ~200-L (~12,000 in^3) airgun source fired every 50 m and a 4-km receiver array with 156 channels. The record lengths were 13.5 s. In this study, we used the data from line SR101 (cruise KR97-07) and lines MY101 and MY102 (cruise KR99-08) in the northern half of the rupture region (38–39°N, red lines in Fig. 1). The location of line MY102 corresponds to the region of significant seafloor uplift as estimated by tsunami inversion (Fujii et al., 2011; Tsuji et al., 2011). The locations of lines MY101 and SR101 are northern edge and outside of the seafloor uplifted region, respectively.

Seismic processing (Yilmaz, 2001) included trace editing, multiple suppression, deconvolution, velocity analysis, stacking, post-stack migration, and spherical divergence correction. Fig. 2 shows the seismic profiles converted to depth on the basis of stacking velocities. Seismic velocities and accurate depths of reflection events were difficult to determine for the deeper geological units because of the limited streamer length. Therefore, to convert time to depth in the deeper part of the profiles, we used *P*-wave velocities derived from wide-angle refraction analysis (Murauchi and Ludwig, 1980; Suyehiro and Nishizawa, 1994). For seismic line SR101, prestack-depth migration was applied (Tsuru et al., 2002).

2.2. Seafloor observations

Before the earthquake, we used the manned submersible *Shinkai 6500* (e.g., cruise YK08-06 in 2008) to deploy seafloor observatories close to fault traces identified on seismic reflection profiles (Ito et al., 2011; Tsuji et al., 2011; Fig. 1b). After the earthquake (in June and August 2011, and July and August 2012), we revisited all of the pre-earthquake dive points in the manned submersible (cruises YK11-06E and YK12-13) or with a deep-tow camera system (cruises YK11-04E and YK12-12). Because of frequent aftershocks generated around the diving sites along the MY102 transect (Sites 3E and 3W in Figs. 1 and 2) shortly after the 2011 earthquake (August 2011), we used the deep-tow camera system to investigate those sites instead of the manned submersible. In August 2012, we were able to dive to Site 3E (a region of significant seafloor uplift) in the manned submersible.

For our post-earthquake observations, we tried to dive along the same tracks used for the pre-earthquake observations in order to evaluate changes to the seafloor environment and morphology along those tracks. Because some of the diving stations had moved several tens of meters during the 2011 earthquake (Fig. 1a; Ito et al., 2011; Sato et al., 2011), we needed to take into account the seafloor movements in order to follow the same diving tracks for our post-earthquake observations. Comparison of the seafloor fault traces before and after the earthquake (Figs. 3–6) revealed dynamic changes to the seafloor morphology and environment caused by the 2011 Tohoku-oki earthquake.

After the earthquake, to characterize the seafloor deformation in the wider region of tsunami generation, we undertook dives at two new sites (Sites 2E and 4W in Fig. 1b) that had not been visited before the earthquake. These sites are also located along seafloor traces of dominant faults, identified on seismic reflection profiles as a backstop interface (Site 2E) and a landward-dipping normal fault (Site 4W).

2.3. Heat flow measurements

Along with the post-earthquake seafloor observations, extensive measurements of heat flow were made at the fault traces. Heat flow measurements provide important constraints on the dynamics of fault activity. Because fluids from considerable depth pass through the fault plane (open fracture) generated by a dynamic fault rupture, the degree of fault activity as well as the rupture mechanics directly influence the heat flow measured at overlying seafloor fault traces. Previous studies (Ranero et al., 2008; Davis et al., 2006; Kawagucci et al., 2012; Davis and Villinger, 2006; Solomon et al., 2009; Saffer and Tobin, 2011) have demonstrated a clear relation between seismicity and fluid movement resulting in a temperature anomaly. Frictional heat due to fault rupture also increases heat flow, but that effect is minimal at the seafloor because of the low effective stress across the shallow fault plane. Although changes in seafloor morphology in the submersible observations (e.g., open fissures) constitute direct evidence of dynamic activity, they are often affected by shallow activity such as seafloor slumping. Heat flow data can be used to link seafloor observations with deep structural activity.

Since repeat measurements of heat flow were made at the same stations in 2011 and 2012 (Fig. 3g and h), we can evaluate the timing of fault activity from the heat flow variation after the 2011 earthquake. Following the earthquake, as fault activity decreased, heat flow at the seafloor fault trace would also decrease. Measured heat flow values at some geologic feature

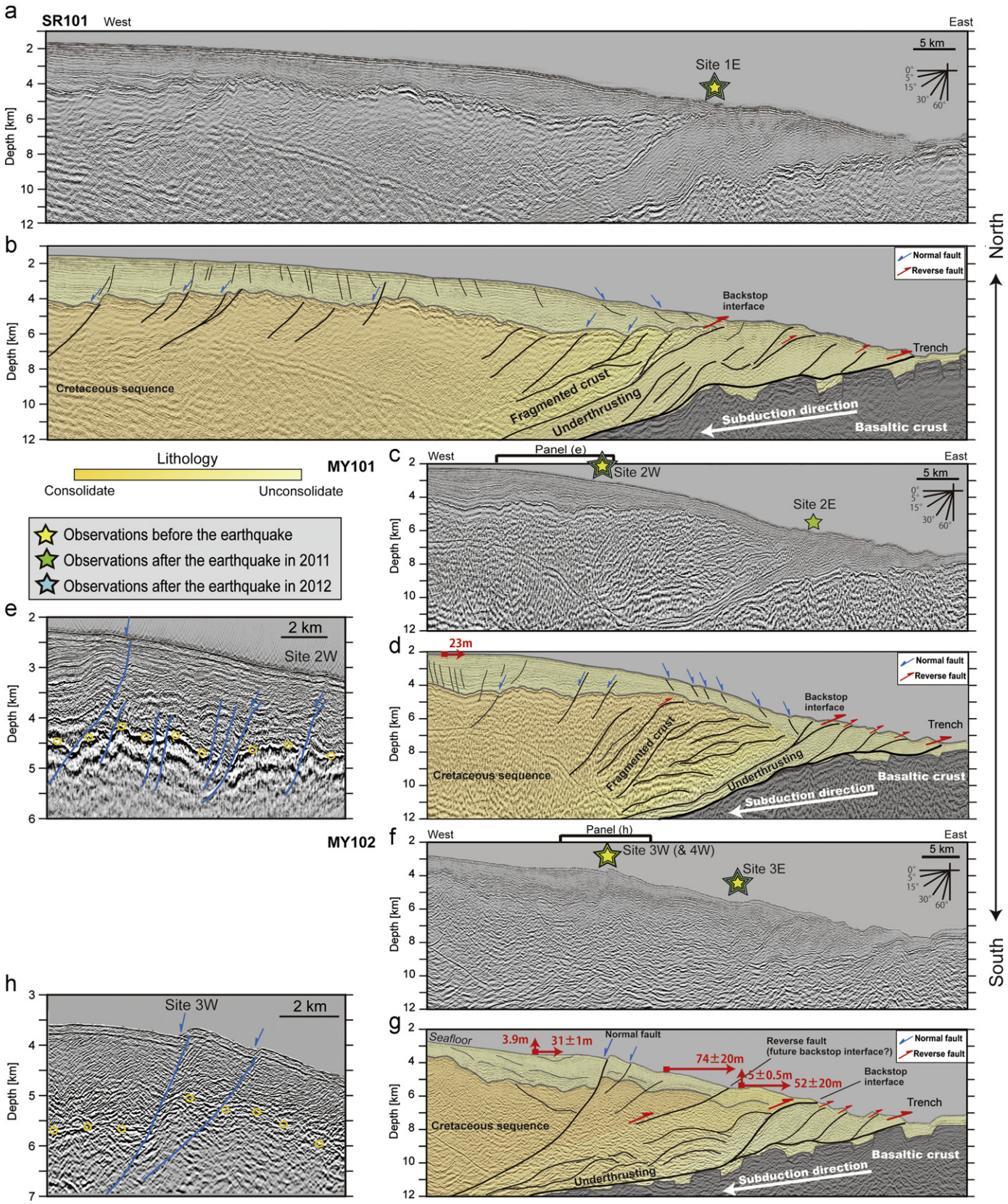

Fig. 2. Reflection seismic profiles obtained in the central part of tsunami source area (line MY102 in panels f–h), at its northern edge (line MY101 in panels c–e), and its outside (line SR101 in panels a, b). Original profiles of (a) line SR101, (c) line MY101, and (f) line MY102. Composite seismic reflection profiles with geological interpretations of (b) line SR101, (d) line MY101, and (g) line MY102 (Tsuji et al., 2011). Red arrows in panel (d) and (g) indicate seafloor displacements (Ito et al., 2011; Kido et al., 2011; Sato et al., 2011). Enlarged profiles around (e) Site 2W on line MY101, and (h) Site 3W on line MY102. (For interpretation of the references to color in this figure legend, the reader is referred to the web version of this article.)

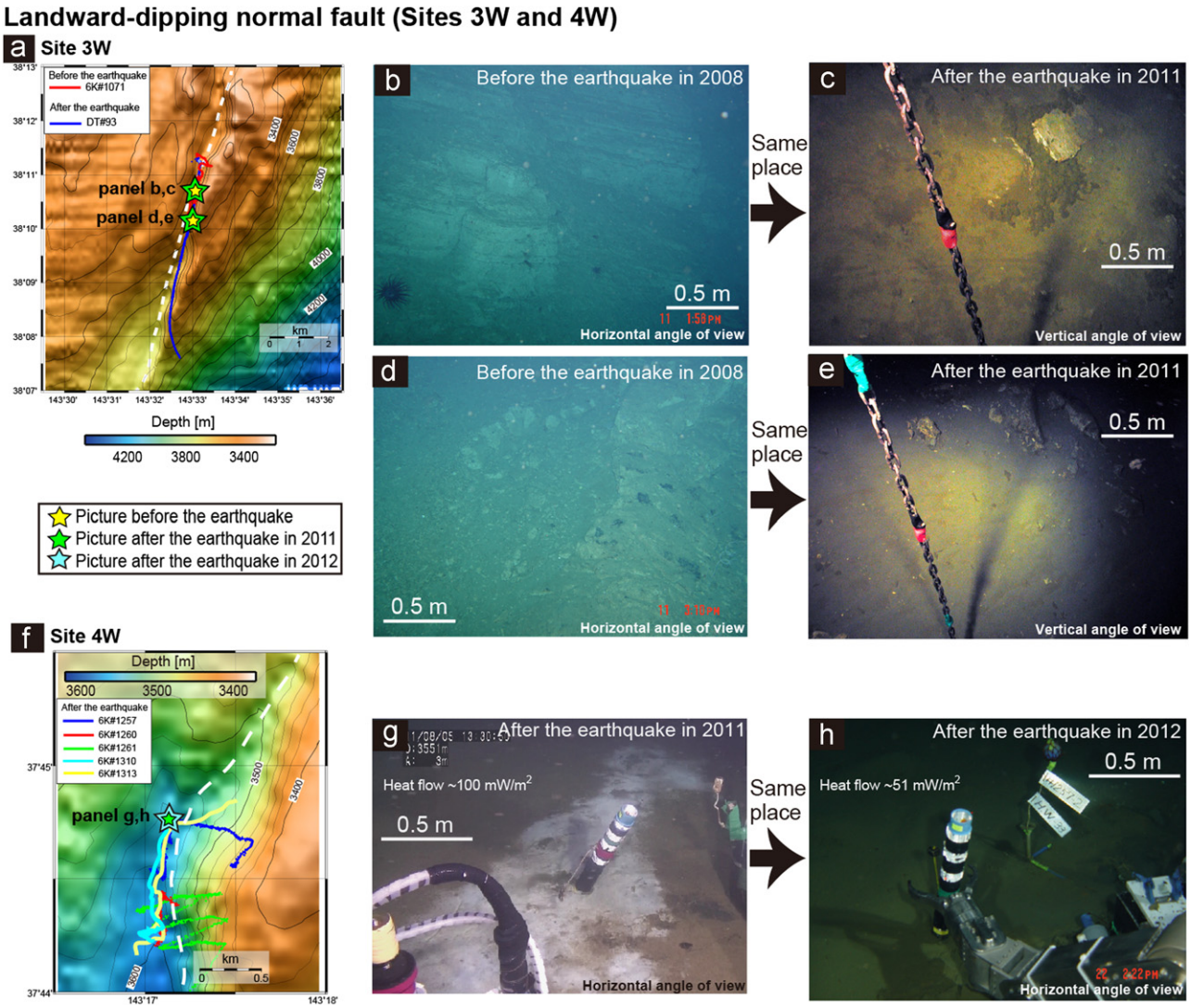

Fig. 3. (a) Diving tracks on seafloor bathymetry at Site 3W. Stars indicate locations of seafloor images displayed in this figure. The white dashed line indicates the location of the interpreted fault. (b–e) Photographs of the cliff generated by normal faulting at Site 3W (b, d) before and (c, e) after the earthquake. (f) Diving tracks on seafloor bathymetry at Site 4W. (g, h) Photographs at Site 4W taken in (g) 2011 and (h) 2012, showing heat flow measurements being made at the same location by SAHF probe.

(e.g., an open fissure) that are low and constant in repeated measurements (in both 2011 and 2012) would suggest that the geologic feature is related to some small-scale (regional) phenomenon.

The vertical thermal gradient was measured by inserting a Stand-Alone Heat Flow (SAHF) probe into the seafloor by using the arms of the manned submersible. The SAHF probe is 60 cm long with five thermistors mounted at intervals of 11–12 cm along the probe. We usually measured thermal gradients over ~20 min at each measurement station. However, at two measurement stations within Site 1E (Fig. 1), we measured the thermal gradient over ~48 h to obtain heat flow values with higher accuracy.

In the laboratory, we measured the thermal conductivity of the mudstone and core samples obtained at almost all of the heat flow measurement stations. The measured thermal conductivity ranged from 0.68 to 0.91 W/mK. In this study, we used 0.88 W/mK as the thermal conductivity to be consistent with a previous heat-flow study (Yamano et al., 2008) in this region. From the thermal gradient (mK/m) and the thermal conductivity (W/mK), we calculated heat flow values (mW/m^2) at each measurement point (Table 1, Fig. 7).

3. Results and interpretation

3.1. Fault characteristics observed in seismic reflection profiles

On all seismic reflection profiles acquired across the Japan Trench (Fig. 2), we identify the subducting Pacific Plate and the plate interface as strong reflections. Several faults are interpreted to branch up from the plate interface. However, the reflective characteristics of the fault system within the overriding plate are different between seismic profiles acquired within and outside of the tsunami source area. Features related to the backstop interface and underthrusting sequence especially differ between the seismic profiles from the two areas (Fig. 2).

3.1.1. Central part of the tsunami source region (line MY102)

On the seismic reflection profile closest to the tsunami source area off Miyagi (line MY102 in Figs. 1, 2f and g), a large landward-dipping normal fault within the continental crust is located ~40 km landward from the trench axis (Tsuji et al., 2011). Several additional normal faults can be identified close to this fault. Accumulated

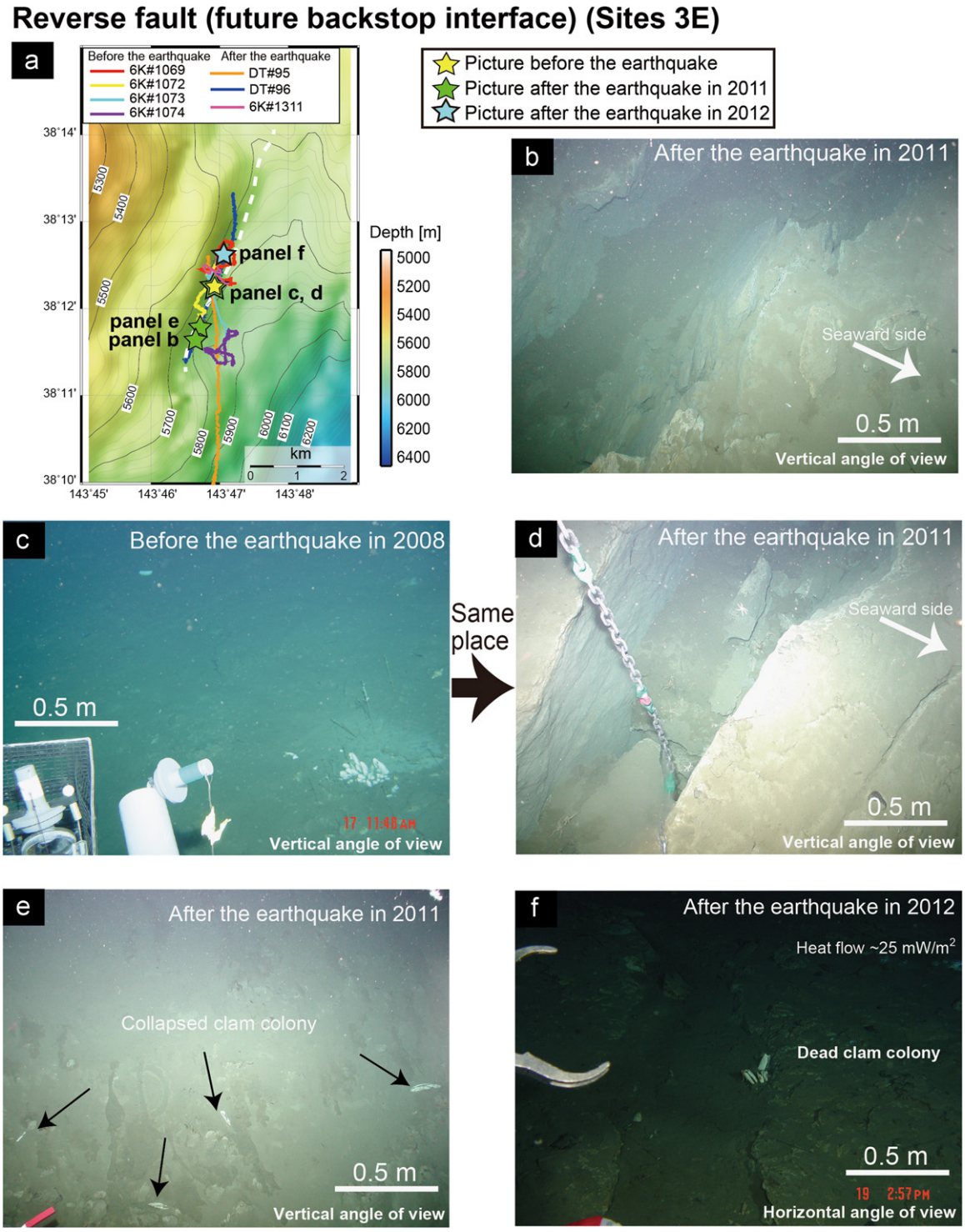

Fig. 4. (a) Diving tracks on seafloor bathymetry at Site 3E. The white dashed line indicates the location of the interpreted fault. Stars indicate locations of seafloor photographs displayed in panels (b)–(f). (b) Photograph of an open fissure representative of those commonly observed after the earthquake. (d) Post-earthquake observations revealed open fissures along the interpreted fault trace where (c) clam colonies were observed before the earthquake. (e) Clam colonies collapsed during the 2011 earthquake. (f) Only one clam colony was observed at this site after the earthquake, but all clams were dead.

displacement on the large normal fault is significant; the offset of the Cretaceous sequence is estimated to be 800 m, and the ridge at the seafloor is ~150 m high (Fig. 2h). The difference between the smaller seafloor and the larger basement displacements may reflect the accumulated offset of multiple earthquakes. Furthermore, the existence of a steep cliff or escarpment along the fault trace at the seafloor (Fig. 3b) indicates that the normal fault is active (Tsuji et al., 2011). The chemical composition of the water at the seafloor along seismic line MY102 (Fig. 2f), measured after the earthquake, demonstrates that seepage from relatively deep units occurred only on the landward side of the normal fault (Kawagucci et al., 2012), suggesting that the fault acts as a hydrological boundary that divides the continental margin framework.

Although we cannot clearly identify reflections from the deeper part of this fault, the large displacement along the normal fault (~800 m) suggests that it branches up from the top of the

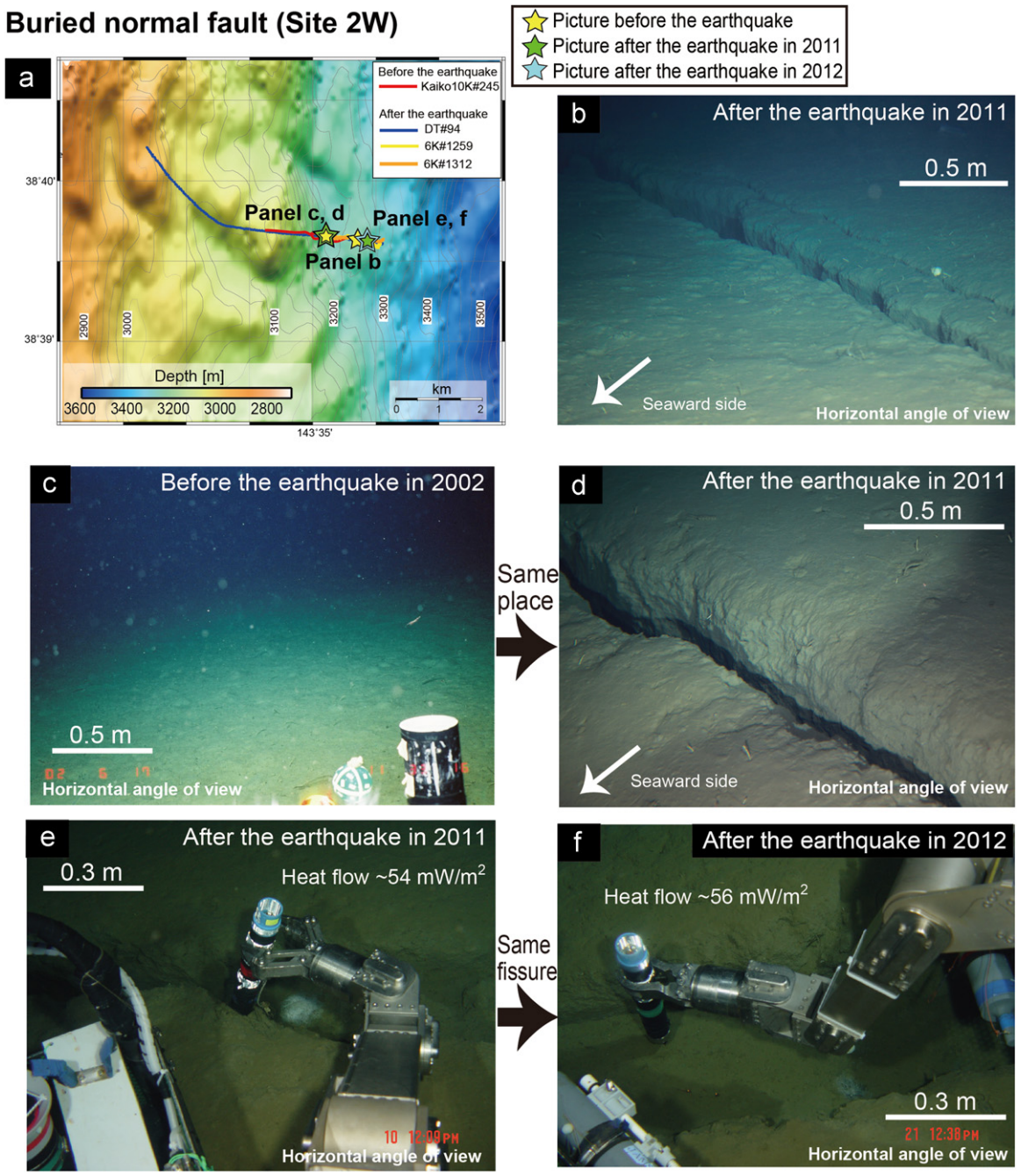

Fig. 5. (a) Diving tracks on seafloor bathymetry at Site 2W. Stars indicate locations of seafloor photographs displayed in panels (b)–(f). (b) Photograph of an open fissure representative of those commonly observed after the earthquake. (d) An open fissure was observed during post-earthquake observations where (c) no fissure had been before the earthquake. (g, h) Photographs taken in (g) 2011 and (h) 2012 showing the heat flow measurements being made at the same location by SAHF probe.

underthrusting sequence or plate interface (~5 km deeper than the continental crust surface). Indeed, Conin et al. (2012) showed that normal faulting along a fault branched from a plate interface (i.e., a landward-dipping normal fault) is possible if the friction along the seaward plate interface is low during the coseismic rupture.

On the southern side of line MY102 (Fig. 1b), several seafloor ridges oriented parallel to the trench axis and attributable to this normal fault displacement are located where the seafloor slope steepens seaward. Seismic reflection data acquired after the 2011 earthquake indicate that the landward-dipping normal fault runs beneath the ridge structure observed on the southern side of line MY102, and as such, is a prominent structure in the tsunamigenic region. Numerous normal-fault aftershocks in the overriding plate (Asano et al., 2011) further indicate that the extensional faults imaged on the seismic profile ruptured during the 2011 earthquake.

The 2011 Tohoku-oki earthquake caused considerable horizontal seafloor displacement (Fujiwara et al., 2011) and extension around the large normal faults (Ito et al., 2011); one seafloor observatory was moved >50 m seaward of the normal fault, and another one on the landward side of the fault was moved ~30 m in the seaward direction (Fig. 2g). Ruptures on a series of normal faults account for the large extensional stress between these two observatories (extensional strain $>10^{-3}$; Ito et al., 2011). Because the dip angle of the normal faults ($<45^{\circ}$) is not steep for a normal

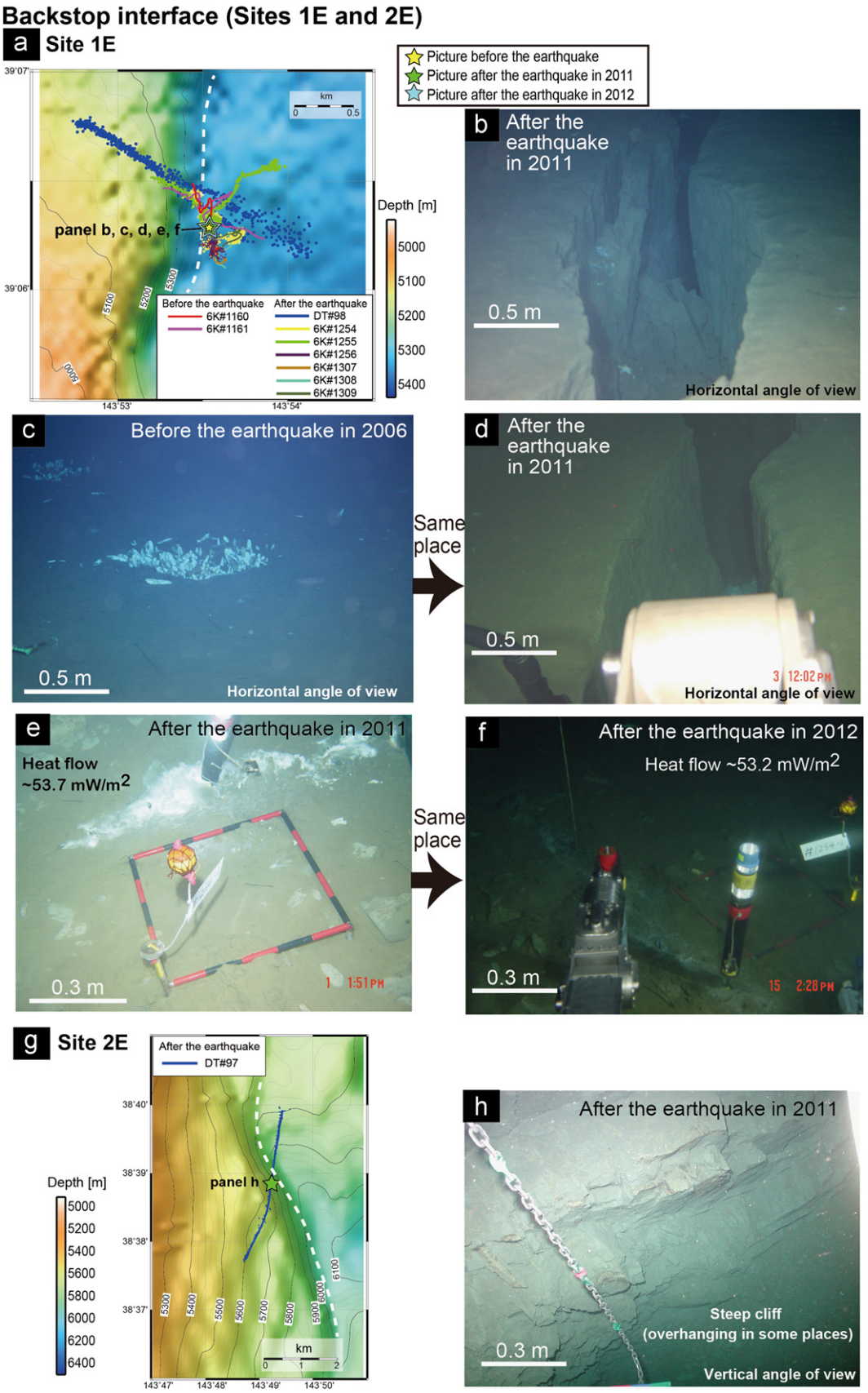

Fig. 6. (a) Diving tracks on seafloor bathymetry at Site 1E. The white dashed line indicates the location of the interpreted fault. Stars indicate locations of seafloor images displayed in panels (b)–(f). (b) Photograph of an open fissure representative of those commonly observed after the earthquake. (d) Open fissure seen during post-earthquake observations where (c) a clam colony (~1 m wide) was observed before the earthquake. (e, f) Photographs taken in (e) 2011 and (f) 2012, showing the heat flow measurements at the same location by SAHF probe. (g) Dive track on seafloor bathymetry at Site 3E. The star indicates the location of (h) a seafloor photograph showing a steep cliff.

Table 1
Heat flow values measured at Sites 1E, 2W, 3E, and 4W.

Position	Lat.	Lon.	Dep. (m)	Dive	Date	Time	Thermal Gradient (mK/m)	Heat flow (mW/m^2)
Site 1E: 39°N backstop interface								
1E-1	39–6.3315	143–53.5589	5348	#1254	Aug. 01, 2011	13:58	61.023 ± 0.045306	53.7
				#1308	Aug. 15, 2012	14:41	60.461 ± 0.62473	53.2
1E-2	39–6.5602	143–53.8611	5342	#1255	Aug. 02, 2011	12:49	39.463 ± 5.0253	34.7
				#1309	Aug. 17, 2012	13:14	38.680 ± 1.9993	34.0
1E-3	39–6.5602	143–53.8611	5342	#1255	Aug. 02, 2011	12:49	43.743 ± 3.0346	38.5
1E-4	39–6.3433	143–53.6102	5346	#1307	Aug. 13, 2012	13:54	55.647 ± 0.37152	49.0
1E-5	39–6.3436	143–53.5621	5346	#1307	Aug. 13, 2012	14:42	46.899 ± 0.018815	41.3
Site 2W: 38.5°N small landward-dipping normal fault								
2W-1	38–39.2672	143-36.0120	3243	#1259	Aug. 10, 2011	12:09	61.499 ± 0.5785	54.1
				#1312	Aug. 21, 2012	12:20	68.042 ± 0.55445	59.9
				#1312	Aug. 21, 2012	12:40	64.054 ± 1.6427	56.3
2W-2	38–39.3022	143-35.7381	3213	#1312	Aug. 21, 2012	14:37	98.535 ± 0.84205	86.7
2W-3	38–39.3350	143-35.3686	3230	#1312	Aug. 21, 2012	15:35	104.15 ± 1.5245	91.7
Site 3E: 38°N reverse fault								
3E-1	38-12.3686	143-47.0306	5775	#1311	Aug. 19, 2012	14:15	33.162 ± 0.36437	29.2
3E-2	38-12.5906	143-47.0822	5738	#1311	Aug. 19, 2012	15:30	26.959 ± 0.89856	23.7
Site 4W: 37.5°N landward-dipping normal fault								
4W-1	37–44.7583	143-17.1579	3551	#1257	Aug. 5, 2011	14:31	108.55 ± 1.0035	95.5
				#1257	Aug. 5, 2011	14:31	122.24 ± 2.1147	107.6
				#1310	Aug. 18, 2012	15:57	58.652 ± 0.53338	51.6
				#1313	Aug. 22, 2012	14:27	54.251 ± 1.8163	47.7
4W-2	37–44.2123	143-17.0566	3585	#1260	Aug. 12, 2011	12:08	46.412 ± 1.5418	40.8
				#1313	Aug. 22, 2012	12:55	37.133 ± 17.788	32.7
4W-3	37–44.4354	143-17.0903	3582	#1260	Aug. 12,2011	12:55	44.482 ± 11.128	39.1
				#1313	Aug. 22, 2012	13:38	39.485 ± 2.491	34.7
4W-4	37–44.5421	143-17.0554	3566	#1257	Aug. 5, 2011	11:40	91.649 ± 7.5792	80.7
4W-5	37–44.3662	143-16.9859	3577	#1261	Aug. 13, 2011	10:29	43.581 ± 2.426	38.4
4W-6	37–44.2447	143-17.0322	3585	#1310	Aug. 18, 2012	13:25	58.732 ± 0.59495	51.7
4W-7	37–44.7464	143-17.1697	3553	#1313	Aug. 22, 2012	15:14	58.235 ± 2.1314	51.2

fault, horizontal extension can occur with relatively small displacements along these faults. Moreover, the traces of the large normal faults coincide with the landward edge of the region of significant seafloor uplift (Fujii et al., 2011) and the zone of large displacement (Maeda et al., 2011; Iinuma et al., 2012) (Fig. 1b). These observations suggest that extensional features are dominant in the region where the large normal faults are observed (~40 km landward from the trench) to be associated with the large slip along the plate interface near the trench. Although in an analysis based on differential seafloor bathymetry data, Kodaira et al. (2012) recently reported almost no extension in the region of the normal faults, the resolution of their analysis was lower than 20 m on the landward side of the normal faulting, where the seafloor slope is not steep (Fig. S2 in Kodaira et al. (2012)). From the differential seafloor bathymetry data, therefore, it is difficult to evaluate ruptures along the series of normal faults.

For the vertical displacement, the seafloor seaward of the huge normal fault has been uplifted by ~5 m (Ito et al., 2011) and the landward seafloor has been uplifted by ~3.9 m (Kido et al., 2011) (Fig. 2g). Since one movement of the normal fault cannot explain the magnitudes of both the vertical (~1.1 m) and horizontal (>20 m) relative displacements between these two stations, a number of normal faults distributed around the large normal fault are also likely to have ruptured during the earthquake and thus to have also contributed to the significant horizontal extension in this region.

Several additional faults, including the backstop interface, which is interpreted as the boundary between an accreted unconsolidated sequence (or soft fractured sequence) on the seaward side and a less-deformed Cretaceous sequence (with greater strength) on the landward side, are also visible in this section (von Huene et al., 1994; Tsuru et al., 2002; Fig. 2g). Reflections observed landward of the backstop interface suggest that a sequence has been underthrust beneath the interpreted Cretaceous sequence (Fig. 2g), similar to lens structures observed at other convergent margins (Ranero and von Huene, 2000; Ranero et al., 2000). The consolidated Cretaceous sequence (i.e., continental crust) covering these soft underthrusting sediments would be expected to generate overpressure within the unconsolidated sequence because of compaction equilibrium. Furthermore, clay dehydration would also contribute to overpressure around the plate interface (Kimura et al., 2012). This high pore pressure might weaken coupling along the plate interface.

A reverse fault can be interpreted to exist at the seafloor slope break between the backstop interface and the large normal fault (~20 km from the trench axis; Site 3E in Fig. 2f). In the future, this fault may act as a backstop interface, because an underthrusted sequence is identified on the footwall of this fault and because the fault imaged on seismic line MY102 is at the southern extension of the backstop interface observed in the northern region (yellow dashed line in Fig. 1b).

3.1.2. Northern edge of the tsunami source area (line MY101)

On a seismic reflection profile in the northern edge of the tsunami source area (line MY101, Figs. 1, 2c and d), the fault distribution is different from that off Miyagi (line MY102; Fig. 2f and g). The backstop interface and the underthrusted sediments are clearly imaged beneath line MY101. Several normal faults can be identified along line MY101, but the total amount of displacement of each normal fault is less than that along line MY102 (in the central part of the tsunami source area).

Seaward-dipping normal faults, possibly generated by submarine landslides, are developed around the backstop interface. At the backstop interface, where the margin framework rock is in contact with the frontal prism, it is common to see a steeper slope

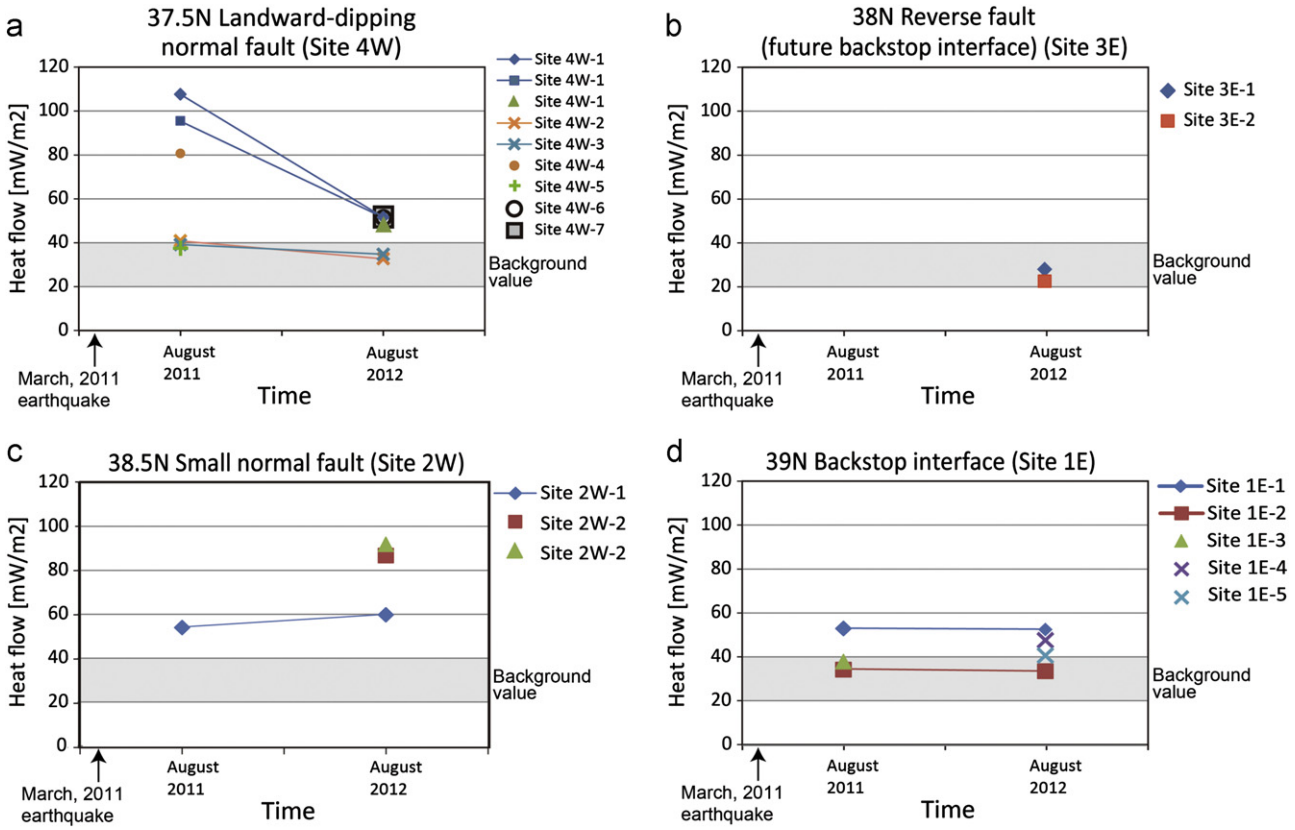

Fig. 7. Time variance of heat flow measured at (a) Site 4W, (b) Site 3E, (c) Site 2W, and (d) Site 1E. (a) Although high heat flow was measured at the landward-dipping normal fault just after the 2011 earthquake, the heat flow decreased to a normal value in 2012. (b) Heat flow values measured at an open fissure above the reverse fault were low compared to those obtained at other measurement sites. (c) Heat flow was constant or increased at the buried landward-dipping normal fault at the northern edge of the tsunami source area. (d) Heat flow was the same in 2011 and 2012 at the backstop interface at the outside of the tsunami source area.

at the edge of the continental framework rock because of the greater strength of the continental framework (yellow dashed line in Fig. 1b). Therefore, seafloor slumping may occur frequently at the steep slope at the backstop interface. Submarine sliding of sediment masses represented by the seaward-dipping faults may have contributed to the tsunami generation (Kawamura et al., 2012), even without any large displacement along the plate interface in this northern part of the rupture area.

3.1.3. *Outside of the tsunami source area (line SR101)*

Fault characteristics observed in the northernmost profile SR101 (Figs. 1, 2a and b) are similar to those in line MY101. However, the horizontal length of the soft frontal prism (from trench axis to backstop interface) is longer than on the southern transects (lines MY101 and MY102), and the backstop interface (i.e., front of the continental crust) is farther landward (Tsuru et al., 2002). The greater width of the sedimentary prism (greatly eroded continental crust) may be related to the location of this seismic line at the outside of the tsunami generation area, as described later. Along seismic line SR101 (Fig. 2a and b), we can identify landward-dipping normal faults distributed on the continental crust surface, but displacement on these faults has not significantly deformed the seafloor, indicating that they are relatively inactive.

3.2. *Seafloor observations and heat flow*

3.2.1. *Landward-dipping normal fault in the central part of the tsunami source area (Sites 3W and 4W)*

Seafloor observations before the 2011 earthquake demonstrated that the seafloor ridge associated with the large normal fault in the source region of the 2011 tsunami (Site 3W in Fig. 1b) is a near-vertical continuous scarp that is overhanging in places (Tsuji et al., 2011) (Fig. 3b). The hard, lithified sediment of the scarp indicates that the deep lithology crops out there as a result of the normal fault displacements. After the 2011 earthquake, the seafloor was covered with layers of soft diatomaceous sediments and greenish fluff floating just above the seafloor (Fig. 3c and e). These sediments were presumably derived from the seafloor slope landward of the ridge and deposited during or after the earthquake, because before the earthquake, the seafloor was covered by gravels from the scarp (Fig. 3b and d). Because of aftershock activity around this site (3W), manned submersible dives were not possible in 2011. However, manned submersible dives were undertaken further south along the seafloor trace of the normal fault at Site 4W (Fig. 1b). Therefore, we measured heat flow along the interpreted normal fault trace at Site 4W (Fig. 3g and h).

Heat flow values measured five months after the earthquake at Site 4W ranged from 33 to 108 mW/m^2 (Figs. 3g, h and 7a). Although heat flow was measured at an undisturbed location on the seafloor (i.e., a location that was not fissured), the high end of this heat flow range is significantly greater than the background values measured before the earthquake (20–40 mW/m^2; Fig. 1a; Yamano et al., 2008, 2010), suggesting that seepage had occurred along the normal fault as a result of dynamic rupture of the fault. Heat flow was also measured within and adjacent to some identified bacterial mats (white-colored spots), but we did not observe significant differences in heat flow values between those measured within and outside the bacterial mats.

The spatial variation of heat flow values at Site 4W (~2 km horizontally; Table 1) can be roughly explained by the distance of each measurement site from the fault scarp. We confirmed that the

site where the highest heat flow was measured was near (<80 m from) the cliff. Because the landward-dipping normal fault should extend beneath the flank of the cliff, the sites with the highest heat flow values (Fig. 3f and g) are those near the seafloor trace of the fault.

Markers deployed during the collection of the heat flow measurements in 2011 allowed repeat measurements to be made at the same locations (<1 m error) in 2012 (Fig. 7a). In August 2012 (17 months after the 2011 earthquake), heat flow at the measurement station where the highest heat flow value had been observed in 2011 (~108 mW/m^2; Fig. 3g) had decreased to the normal background value (~58 mW/m^2; Fig. 3h). The time variation of the heat flow values clearly suggests impulsive fluid movement along the normal fault during the 2011 earthquake.

3.2.2. Reverse fault (future backstop interface) in the central part of the tsunami source area (Site 3E)

Prior to the earthquake, chemosynthetic communities were observed along the reverse fault seafloor trace (Site 3E in Fig. 1b), suggesting seepage along the fault zone (Tsuji et al., 2011) (Fig. 4c). Our post-earthquake observations revealed open fissures (<3 m wide) along the interpreted fault trace (parallel to the strike of the fault; Fig. 4d) where clam colonies had been observed before the earthquake (Fig. 4c). These fissures were not observed before the earthquake. Because no other large earthquake occurred between the 2008 and 2011 seafloor observations and because no large aftershock was observed near the frontal region on the seaward side of the large normal fault (Obana et al., 2012), we consider the 2011 earthquake to be the most likely cause of these fissures. Furthermore, the seafloor geodetic data (Ito et al., 2011, in press; Iinuma et al., 2012) indicate no significant seafloor displacement around Site 3E just before and after the 2011 earthquake, suggesting that the fissures were generated during the mainshock. The configuration of almost all of the dead *Calyptogena* (thermogenic bivalves) found adhering to open cracks or under fallen rocks suggests intensive seafloor sediment flow (Fig. 4e).

On the basis of the seafloor morphology and fault geometry identified from seismic profiles near Site 3E, we previously interpreted this fault as a reverse fault or a future backstop interface (Fig. 2g; Tsuji et al., 2011). However, during the post-earthquake seafloor observations, we found no evidence of reverse fault displacement and instead detected only extensional features. It is possible that the open fissures were generated by seafloor landsliding, but in our observations, including in the deep-tow sub-bottom profiler surveys, we could not find clear evidence of small-scale submarine landsliding at this site.

Heat flow values measured at an open fissure of Site 3E in August 2012 were significantly low (~25 mW/m^2) compared with heat flow at the other observation sites (Fig. 7b) and lower than the background value (Yamano et al., 2010), even though it is probable that the open fissure was formed during the 2011 earthquake and clam colonies suggesting fluid seepage were observed before the earthquake. Because we observed dead clam colonies during the 2012 observations (Fig. 4f), seepage along the fault may have decreased after the 2011 earthquake. Because the stress state within the overriding plate was abruptly changed from compression to extension during the 2011 earthquake (Tsuji et al., 2011; Ito et al., 2011), the hydrological characteristics around the fault would also have been changed by the earthquake.

3.2.3. Small landward-dipping normal faults in the northern edge of the tsunami source area (Site 2W)

Small-scale normal faults are identified in the northern part of the tsunami source area (Figs. 1b, 2c and d). At one buried landward-dipping normal fault (Site 2W in Fig. 1b) where submersible surveys were conducted both before and after the 2011 earthquake, we confirmed the development of open fissures (Fig. 5d) not observed before the earthquake (Fig. 5c), and which therefore likely resulted from the earthquake. Because the seafloor is lower on the seaward side of some of these fissures than on the landward side (Fig. 5d), the fissures may have formed by gravitational failure (Kawamura et al., 2012).

Heat flow of ~54 mW/m^2 at an open fissure above the buried landward-dipping normal fault (Site 2W) measured just after the earthquake in 2011 (Fig. 5e) was not much higher than the background value (Yamano et al., 2010). Furthermore, the heat flow measured at this station (Fig. 5e and f) was almost the same in both 2011 and 2012 (Fig. 7c), suggesting that significant fault activity did not occur at this location during the earthquake. The open fissure may thus have been generated by small-scale seafloor slumping.

We measured a high heat flow value at a different measurement location at Site 2W in August 2012 (Fig. 7c), but this abnormal heat flow cannot be interpreted on the basis of only one measurement. We plan to measure heat flow at this location again in the near future to investigate further possible activity of the buried normal fault.

3.2.4. Backstop interface at the outside of the tsunami source area (Sites 1E and 2E)

At the backstop interface at the outside of the tsunami source area (Site 1E in Fig. 1b; 39°N), where submersible surveys were conducted before the 2011 earthquake, open fissures (Fig. 6b and d) that were not evident before the earthquake (Fig. 6c) were identified during post-earthquake observations, and we assume that they were generated during the 2011 earthquake. The heat flow of 34–54 mW/m^2 measured at the backstop interface after the earthquake is not much higher than the background values (Yamano et al., 2010). Furthermore, the heat flow values measured at the same site after the earthquake in 2011 and in 2012 (Fig. 6e and f) are very similar: 53.7 mW/m^2 in 2011 (Fig. 6e) and 53.2 mW/m^2 in 2012 (Fig. 6f) at the same small fissure, and 39.463 mW/m^2 in 2011 and 38.68 mW/m^2 in 2012 at the same undisturbed seafloor location (Fig. 7d; Table 1). Therefore, the earthquake rupture may not have propagated to the seafloor along the backstop interface at this location. The open fissure may instead be related to small-scale failure (e.g., seafloor landsliding).

During the post-earthquake observations at this location, we observed ballast from the submersible Shinkai 6500 deployed before the earthquake. The depth of the ballast was unchanged between the pre- and post-earthquake observations. Note that the depth accuracy of the manned submersible, as measured by a Paroscientific Inc. SBT13000-I depth sensor, is 0.01%. This corresponds to ~0.53 m (=5300 m × 0.0001) in this region. By additionally considering the error caused by the tide in this region (<1 m), the seafloor at this site could not have moved more than 1.5 m in the vertical direction during the 2011 earthquake. This result is consistent with the seafloor deformation characterized by tsunami inversion methods (Fujii et al., 2011).

At the backstop interface at Site 2E, which was not examined before the earthquake (Fig. 1b), the deep-tow system detected *Calyptogena* at the steep cliff (Fig. 6g), suggesting that seepage has occurred along the backstop interface (i.e., fluid has been squeezed from the underthrusting sequence). Although the steep cliff was found to be overhanging in some places (Fig. 6h), we could not find any clear seafloor deformation (e.g., open fissures) associated with the 2011 earthquake.

4. Discussion

We have used both seafloor observations (Figs. 3–6) and fault distributions interpreted on seismic reflection profiles (Fig. 2) to

assess the generation mechanisms of the huge 2011 tsunami. On the basis of the post-earthquake seafloor observations, where we observed open fissures at almost all observation points, we have proposed anelastic deformation above the plate interface. Furthermore, abnormal heat flow at a landward-dipping normal fault suggests normal fault rupture in this region during the 2011 earthquake. These observations help us to understand the mechanisms of tsunami generation.

Here we compare fault distributions in the central (line MY102) and northern (lines MY101 and SR101) parts of the tsunami source area in order to further investigate the characteristic structures of the tsunamigenic region. Then, by considering the large-scale structures on the seismic profiles together with the results of the seafloor observations we infer the mechanism of tsunami generation by the 2011 earthquake. Finally, we compare our findings with other tsunamigenic convergent margins where normal faults are preset.

4.1. Characteristic structures in the tsunami source area

Our repeated seafloor observations clearly demonstrate that extensional features commonly observed in the erosional margins were generated coseismically during interplate earthquakes (e.g., the 2011 the Tohoku-oki earthquake), as proposed by Wang and Hu (2006). Because these coseismic extensional processes (which resulted in the normal faulting and open fissures observed in this study) collapse the margin framework into small fragments, they play a vital part in erosion and mass wasting (e.g., von Huene et al., 2004). On the seismic profiles (Fig. 2), we can recognize fragmented continental units that, together with the soft sediments, are underthrusting beneath the continental crust along with the subducting Pacific Plate. However, the characteristic geologic structures and the fault distributions around the backstop interface are different between the central part (line MY102) and the northern edge (and outside; lines MY101 and SR101) of the tsunami source area (Figs. 1, 2, and 8).

At the northern edge (and outside) of the huge tsunami source area (lines MY101 and SR101; Fig. 1), the continental crust is collapsing in the transition zone between the frontal prism and continental basement (i.e., at backstop interface) (Figs. 2a–d and 8a). This transition zone can be identified from seafloor bathymetry as a steep slope (yellow dashed line in Fig. 1b), suggesting that the collapse of the consolidated continental framework occurred mainly at the backstop interface.

However, on line MY102, where the huge tsunami was generated during the 2011 earthquake, extensional faulting around a large landward-dipping normal fault, ~30 km landward from the backstop interface (~40 km landward from the trench), seems to collapse the continental framework and detach the seaward frontal crust from the landward crust (Figs. 2f, g and 8b). As a result of this extension, a basin structure has developed on the landward side of the large normal fault (Fig. 2f and g). Since the continental crust is being smoothly displaced in the seaward direction by the movement of a series of normal faults (i.e., dislocation planes), the continental crust on the seaward side of the large normal fault is being continuously re-distributed toward the seaward region close to the trench axis. As a result, the backstop interface is near the trench (~10 km from the trench axis) off Miyagi (line MY102), where the large plate-boundary slip was generated. This feature, which is distinct from the situation in the northern region, is clearly evident from the seafloor bathymetry; in the tsunami source area, a steep seafloor slope is not observed around the backstop interface (yellow dashed line in Fig. 1b), suggesting that the extension of the continental crust occurred gradually. Tsuru et al. (2002), by examining many seismic reflection profiles across the Japan Trench, previously showed that off Miyagi continental crust is found close to the trench axis. In the tsunami source area off Miyagi, where continental crust is close to the trench, the axis of the Japan Trench exhibits a convex seaward curvature (Fig. 1). It is possible that this curvature of the trench axis is related to the gradual extension of continental framework associated with the series of normal faults.

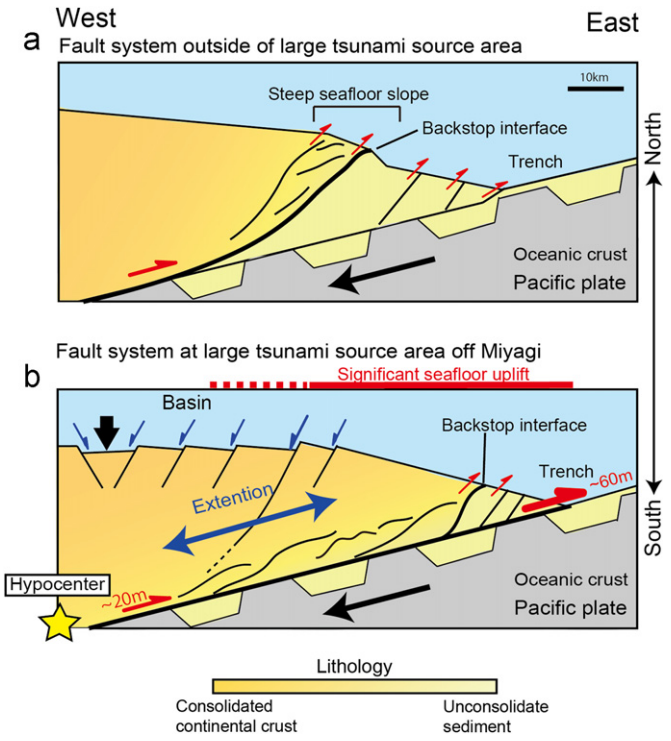

Fig. 8. Schematic images of coseismic fault ruptures and the tsunami generation model (a) at the northern edge (and outside) and (b) in the central part of the tsunami source area. Soft slope sediments covering the continental crust are not shown in these images. (a) Collapse of the continental framework occurred mainly at the backstop interface north of the large tsunami source area. (b) Anelastic deformation around the normal fault allowed large extension of the overriding plate in the tsunami source area.

This interpretation is supported by the small number of aftershocks that were observed within the frontal prism on the seaward side of the large normal fault (Obana et al., 2012), which suggests that the frontal part of continental crust moved seaward without strain accumulation during the coseismic period. During the interseismic period, in contrast, the presence of the continental crust near the trench may allow strain accumulation along the plate interface; therefore, the presence of rigid basement rock close to the trench may contribute to coseismic rupture near the trench (Ryan et al., 2012).

The seaward extension of continental crust may be a characteristic feature of tsunamigenic earthquakes. Kanamori and Kikuchi (1993) suggested that the absence of sediments near the trench (i.e., seaward extension of continental crust) allows the slip to propagate all the way to the trench during a tsunamigenic earthquake. Therefore, the existence of a large normal fault that moves the continental framework seaward should be a key structure characterizing rupture near the trench.

4.2. Dynamic tsunami mechanism of the 2011 earthquake

During most interplate earthquakes, the rupture generated at the deep plate interface does not propagate to the trench, possibly because of the presence of a soft sedimentary prism near the trench (Kanamori and Kikuchi, 1993). As a result, seafloor uplift is

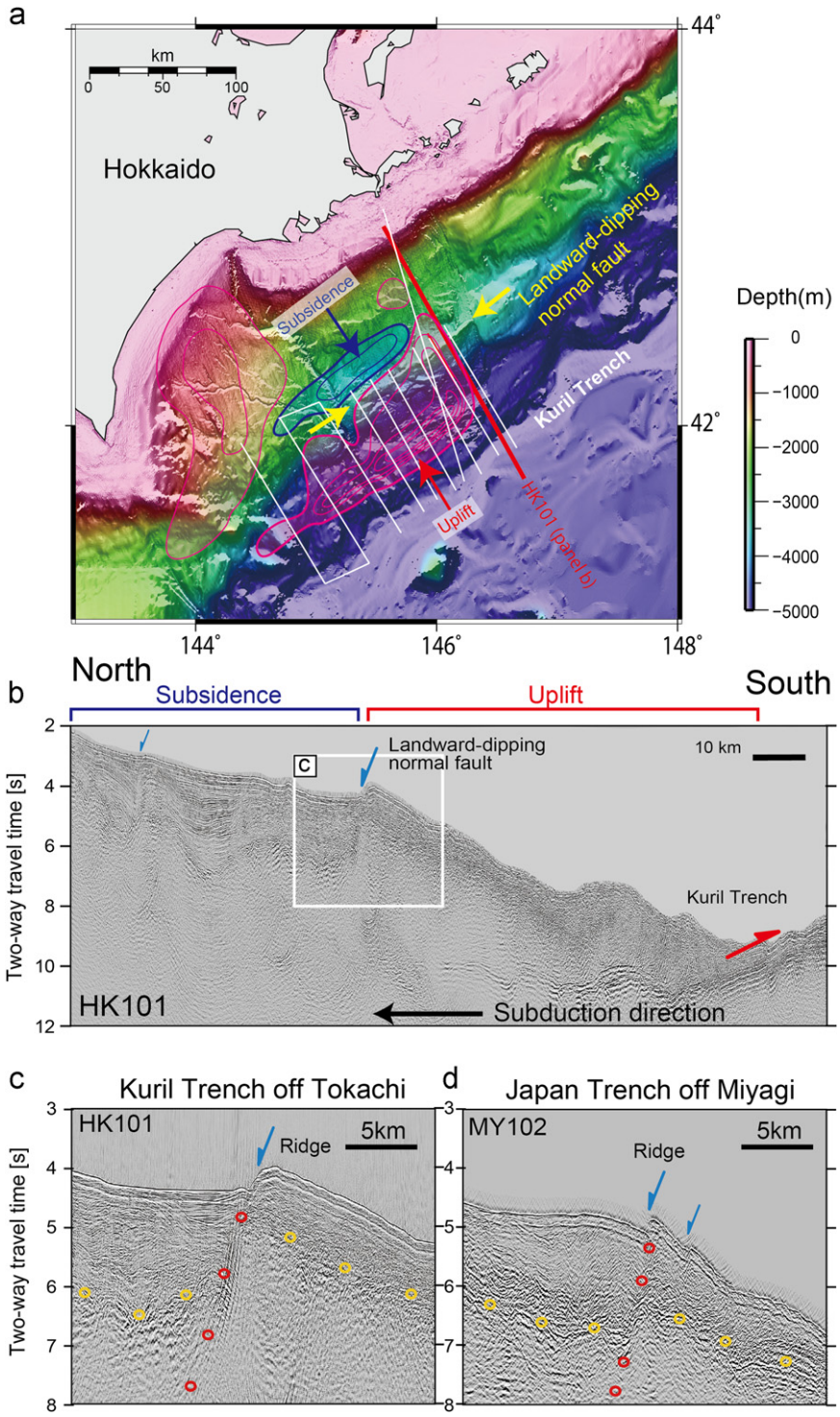

Fig. 9. Similar normal fault in the Kuril Trench, in the tsunami source area of the 1952 Tokachi-oki earthquake. (a) Index map. Red and blue areas indicate areas that uplifted and subsided, respectively, during the 1952 earthquake (Hirata et al., 2003). White lines are the locations of seismic lines that image normal faults (Okamura et al., 2008). (b) Landward-dipping normal faults observed in a time-domain seismic reflection profile acquired in the Kuril Trench (line HK101) (Nakanishi et al., 2004). The location of this seismic profile is shown by a red line in panel (a). The linear ridge structure caused by normal fault displacement (yellow arrows in panel a) coincides with the boundary of the uplift (red) and subsidence (blue) areas during the 1952 Tokachi-oki earthquake. The seafloor depth of the linear ridge is similar to the depth of the seafloor ridge in the Japan Trench. (c) Detailed time-domain seismic profile around the seafloor trace of normal fault (red dots) in the Kuril Trench (line HK101). (d) Detailed time-domain seismic profile around the seafloor trace of the normal fault (red dots) in the Japan Trench off Miyagi (line MY102).

less and a smaller tsunami is generated in the rupture mechanism. During the 2011 earthquake, however, the displacement along the plate interface propagated to the trench axis (Fig. 8b) (Ide et al., 2011; Fujiwara et al., 2011; Kodaira et al., 2012). Furthermore, since the displacement near the trench was greater than at the deeper plate interface (Ito et al., 2011), the normal faulting and opening of fissures (anelastic deformation) observed on the seafloor (Figs. 3–6) correspond to seafloor rupturing caused by extension of the overriding plate (Tsuji et al., 2011). Because anelastic deformation has collapsed the continental crust

framework around the large normal fault in the tsunami source area (~30 km landward of the backstop interface; Fig. 8b), greater extension of the overriding plate was possible, leading to the greater slip (~60 m) along the plate interface near the trench.

This slip contributed significantly to the generation of the tsunami, both because the seafloor slope was steeper on the seaward side of the landward-dipping normal fault (Figs. 1 and 2; Satake, 1994; Tanioka and Satake, 1996) and because the uplifted deep seafloor near the trench (at ~7 km depth) amplified the height of the resultant tsunami (Ryan et al., 2012). Therefore, a large horizontal movement of the steep seafloor near the trench caused significant seafloor uplift and contributed to the displacement of large volumes of water.

4.3. Other tsunamigenic earthquakes

Similar landward-dipping normal faults have been clearly imaged on seismic profiles acquired along the Costa Rica–Nicaragua (Ranero and von Huene, 2000; Ranero et al., 2000), Chilean (Ranero et al., 2006), and Kuril (Okamura et al., 2008) convergent margins. Because of extensional faulting, the continental frameworks are close to the trench axis along all of these convergent margins, and in fact, tsunamigenic earthquakes (long period, large displacements) have occurred at these convergent margins: the 1960 Peru, 1963 and 1975 Kuril Islands, and 1992 Nicaragua earthquakes (Kanamori and Kikuchi, 1993). Aftershocks of tsunamigenic earthquakes in these subduction zones also often have normal fault mechanisms (McKenzie and Jackson, 2012). Therefore, we expect normal faults causing extension of the continental crust should be common structures in regions where tsunamis are generated. Although the mechanisms proposed in this study cannot explain all large tsunamis (e.g., tsunamis generated by seafloor slumping), the extensional features (i.e., the seaward extension of continental crust) may explain the huge tsunami that was triggered by the 1952 Mw 8.1 Tokachi-oki earthquake in the Kuril Trench.

In the Kuril Trench, the northern continuation of the Japan Trench, a similar landward-dipping large normal fault manifests as a continuous ~500-m-high ridge on the seafloor (Nakanishi et al., 2004; Okamura et al., 2008) (Fig. 9). The linear ridge structure is at the seafloor slope break, as in the case of the Japan Trench off Miyagi (Fig. 9c and d). In the Kuril Trench, seafloor deformation near the trench also generated a huge tsunami during the 1952 earthquake (Hirata et al., 2003). Because the location of the large normal fault is coincident with the boundary between the seaward uplift region and the landward subsidence region associated with the earthquake (Hirata et al., 2003) (Fig. 9), the huge tsunami may have been generated by mechanisms similar to those that generated the 2011 tsunami. Because of the normal faulting, the continental crust is close to the axis of Kuril trench (Fig. 9). These findings suggest that the existence of normal faults can be considered as one indicator of a huge tsunami source area near the trench.

Because the seafloor on the landward side of the landward-dipping normal fault subsided during the 1952 Tokachi-oki earthquake (Hirata et al., 2003), we suggest that the primary mechanism that generated the huge tsunami during that event was large displacement along the plate interface near the trench caused by the release of gravitational potential energy (McKenzie and Jackson, 2012; Fig. 9c).

5. Summary

The seafloor morphology and environment off Miyagi where the large plate-boundary slip was generated underwent dynamic changes during the 2011 Tohoku-oki earthquake, particularly in proximity to the seafloor traces of an extensive fault system interpreted on seismic reflection profiles. Open fissures and high heat flow observed at large normal fault indicate considerable extension of the overriding plate, leading to a large rupture along the plate interface near the trench. Since extensional faulting within the region of tsunami generation occurred far landward from the backstop interface, the continental crust actually extends to close to the trench axis. These features are distinct from the features observed outside the tsunami source area.

Similar extensional structures are commonly seen at other convergent plate margins where tsunami earthquakes have been generated. In the Kuril Trench, a similar landward-dipping normal fault that moves the continental framework seaward is observed between the middle and lower trench slope. The seaward extension of continental crust can explain the tsunami generated there by the 1952 Tokachi-oki earthquake. Therefore, fault system characteristics (i.e., landward-dipping normal faults) and geological structures within the overriding plate (i.e., continental crust close to the trench) are keys to identifying regions along convergent margins where huge tsunamis might be generated.

Acknowledgments

We thank the shipboard scientists and technical staff of cruises YK08-06, YK11-04E, YK11-06E, and YK12-13 of R/V *Yokosuka* (JAMSTEC). We especially thank K. Arai (Chiba University), and Y. Masaki and W. Tanikawa (JAMSTEC) for their help during the research cruise. Seismic data were acquired by R/V *Kairei* (JAMSTEC). R. von Huene (University of California, Davis), D. Tappin (British Geological Survey) and anonymous reviewer gave us very helpful comments. This study was supported by a Grant-in-Aid for Scientific Research on Innovative Areas from the Japan Society for the Promotion of Science (JSPS) (21107003). T. Tsuji gratefully acknowledges the support of the International Institute for Carbon Neutral Energy Research (WPI-I2CNER), sponsored by the World Premier International Research Center Initiative (WPI), MEXT, Japan.

References

Asano, Y., Saito, T., Ito, Y., Shiomi, K., Hirose, H., Matsumoto, T., Aoi, S., Hori, S., Sekiguchi, S., 2011. Spatial distribution and focal mechanisms of aftershocks of the 2011 off the Pacific coast of Tohoku Earthquake. Earth Planets Space 63, 669–673.

Conin, M., Henry, P., Godard, V., Bourlange, S., 2012. Splay fault slip in a subduction margin, a new model of evolution. Earth Planet. Sci. Lett. 341–344, 170–175.

Davis, E., Becker, K., Wang, K., Obara, K., Ito, Y., Kinoshita, M., 2006. A discrete episode of seismic and aseismic deformation of the Nankai trough subduction zone accretionary prism and incoming Philippine Sea plate. Earth Planet. Sci. Lett. 242, 73–84.

Davis, E., Villinger, H., 2006. Transient formation fluid pressures and temperatures in the Costa Rica forearc prism and subducting oceanic basement CORK monitoring at ODP Sites 1253 and 1255. Earth Planet. Sci. Lett. 245, 232–244.

DeMets, C., Gordon, R.G., Argus, D.F., Stein, S., 1990. Current plate motions. Geophys. J. Int. 101, 425–478.

Fujii, Y., Satake, K., Sakai, S., Shinohara, M., Kanazawa, T., 2011. Tsunami source of the 2011 off the Pacific coast of Tohoku, Japan earthquake. Earth Planets Space 63, 815–820.

Fujiwara, T., Kodaira, S., No, T., Kaiho, Y., Takahashi, N., Kaneda, Y., 2011. The 2011 Tohoku-Oki earthquake: displacement reaching the trench axis. Science 334, 1240.

Grilli, S.T., et al., 2012. Numerical simulation of the 2011 Tohoku tsunami based on a new transient FEM co-seismic source: comparison to far- and near-field observations. Pure Appl. Geophys., http://dx.doi.org/10/1007/s0024-012-0528-y.

Gulick, S.P.S., Austin, J.A., McNeill, L.M., Bangs, N.L., Martin, K.M., Henstock, T.J., Bull, J.M., Dean, S.M., Djajadihardja, Y.S., Permana, H., 2011. Updip rupture of the 2004 Sumatra earthquake extended by thick indurated sediments. Nat. Geosci. 4, 453.

Hayashi, Y., Tsushima, H., Hirata, K., Kimura, K., Maeda, K., 2011. Tsunami source area of the 2011 off the Pacific Coast of Tohoku Earthquake determined from

tsunami arrival times at offshore observation stations. Earth Planets Space 63, 809–813.
Henstock, T.J., McNeill, L.C., Tappin, D.R., 2006. Seafloor morphology of the Sumatran subduction zone: surface rupture during megathrust earthquakes? Geology 34, 485–488.
Hirata, K., Geist, E.L., Satake, K., Tanioka, Y., Yamaki, S., 2003. Slip distribution of the 1952 Tokachi-Oki earthquake (M8.1) along the Kuril Trench deduced from tsunami waveform inversion. J. Geophys. Res. 108, 2196, http://dx.doi.org/10.1029/2002JB001976.
Ide, S., Baltay, A., Beroza, B.C., 2011. Shallow dynamic overshoot and energetic deep rupture in the 2011 Mw 9.0 Tohoku-Oki earthquake. Science 332, 1426, http://dx.doi.org/10.1126/science.1207020.
Iinuma, T., et al., 2012. Coseismic slip distribution of the 2011 off the Pacific Coast of Tohoku Earthquake (M9.0) refined by means of seafloor geodetic data. J. Geophys. Res. 117, B07409, http://dx.doi.org/10.1029/2012JB009186.
Ito, Y., Tsuji, T., Osada, Y., Kido, M., Inazu, D., Hayashi, Y., Tsushima, H., Hino, R., Fujimoto, H., 2011. Frontal wedge deformation near the source region of the 2011 Tohoku-Oki earthquake. Geophys. Res. Lett. 38, L00G05, http://dx.doi.org/10.1029/2011GL048355.
Ito, Y., et al., Episodic slow-slip events in the Japan subduction zone before the 2011 Tohoku-Oki earthquake. Tectonophysics, http://dx.doi.org/10.1016/j.tecto.2012.08.022, in press.
Japan Coast Guard (JCG), Japan Agency for Marine-Earth Science and Technology (JAMSTEC), 2011. Compilation of the Japan Trench bathymetry data collected by Japan Coast Guard and JAMSTEC. Newsl. Seismol. Soc. Jpn. 23, 35–36.
Kanamori, H., 1972. Mechanism of tsunami earthquakes. Phys. Earth Planet. Inter. 6, 246.
Kanamori, H., Kikuchi, M., 1993. The 1992 Nicaragua earthquake: a slow tsunami earthquake associated with subducted sediments. Nature 361, 714–716.
Kawagucci, S., et al., 2012. Disturbance of deep-sea environments induced by the M9.0 Tohoku Earthquake. Sci. Rep. 2, 270, http://dx.doi.org/10.1038/srep00270.
Kawamura, K., Sasaki, T., Kanamatsu, T., Sakaguchi, A., Ogawa, Y., 2012. Large submarine landslides in the Japan Trench: a new scenario for additional tsunami generation. Geophys. Res. Lett. 39, L05308, http://dx.doi.org/10.1029/2011GL050661.
Kerr, R.A., 2011. New work reinforces megaquake's harsh lessons in geoscience. Science 332, 911, http://dx.doi.org/10.1126/science.332.6032.911.
Kido, M., Osada, Y., Fujimoto, H., Hino, R., Ito, Y., 2011. Trench-normal variation in observed seafloor displacements associated with the 2011 Tohoku-Oki earthquake. Geophys. Res. Lett. 38, L24303, http://dx.doi.org/10.1029/2011GL050057.
Kimura, G., Hina, S., Hamada, Y., Kameda, J., Tsuji, T., Kinoshita, M., Yamaguchi, A., 2012. Runaway slip to the trench due to rupture of highly pressurized megathrust beneath the middle trench slope: the tsunamigenesis of the 2011 Tohoku earthquake off the east coast of northern Japan. Earth Planet. Sci. Lett. 339–340, 32–45.
Kodaira, S., No, T., Nakamura, Y., Fujiwara, T., Kaiho, Y., Miura, S., Takahashi, N., Kaneda, Y., Taira, A., 2012. Coseismic fault rupture at the trench axis during the 2011 Tohoku-oki earthquake. Nat. Geosci. 5, 646–650, http://dx.doi.org/10.1038/ngeo1547.
Koper, K.D., Hutko, A.R., Lay, T., 2011. Along-dip variation of teleseismic short-period radiation from the 11 March 2011 Tohoku earthquake (M_w 9.0). Geophys. Res. Lett. 38, L21309, http://dx.doi.org/10.1029/2011GL049689.
Lay, T., Ammon, C.J., Kanamori, H., Xue, L., Kim, M.J., 2011. Possible large near-trench slip during the 2011 Mw 9.0 off the Pacific coast of Tohoku Earthquake. Earth Planets Space 63, 687–692.
Maeda, T., Furumura, T., Sakai, S., Shinohara, M., 2011. Significant tsunami observed at ocean-bottom pressure gauges during the 2011 off the Pacific coast of Tohoku Earthquake. Earth Planets Space 63, 803–808.
McKenzie, D., Jackson, J., 2012. Tsunami earthquake generation by the release of gravitational potential energy. Earth Planet. Sci. Lett. 345–348, 1–8.
Murauchi, S., Ludwig, W.J., 1980. Crustal Structure of the Japan Trench: the Effect of Subduction of Oceanic Crust. Initial Reports of the Deep Sea Drilling Project 56/57, pp. 463–470.
Nakanishi, A., Smith, A.J., Miura, S., Tsuru, T., Kodaira, S., Obana, K., Takahashi, N., Cummins, P.R., Kaneda, Y., 2004. Structural factors controlling the coseismic rupture zone of the 1973 Nemuro-Oki earthquake, the southern Kuril Trench seismogenic zone. J. Geophys. Res. 109, B05305, http://dx.doi.org/10.1029/2003JB002574.
Obana, K., Shinohara, M., Yamada, T., Uehira, K., Hino, R., Shiobara, H., Nakahigashi, K., Sugioka, H., Ito, A., Nakamura, Y., No, T., Miura, S., Kodaira, S., Takahashi, N., 2012. Near-trench aftershocks of the 2011 Tohoku-oki earthquake based on ocean bottom seismograph observations. 2012 AGU Fall Meeting, T21F-05.
Okamura, Y., Tsujino, T., Arai, K., Sasaki, T., Satake, K., Joshima, M., 2008. Fore arc structure and plate boundary earthquake sources along the southwestern Kuril subduction zone. J. Geophys. Res. 113, B06305, http://dx.doi.org/10.1029/2007JB005246.
Ranero, C.R., von Huene, R., 2000. Subduction erosion along the Middle America convergent margin. Nature 404, 748–752.
Ranero, C.R., von Huene, R., Flueh, E., Duarte, M., Baca, D., McIntosh, K., 2000. A cross section of the convergent Pacific margin of Nicaragua. Tectonics 19, 335–357.
Ranero, C.R., von Huene, R., Weinrebe, W., Reichert, C., 2006. Tectonic Processes along the Chile Convergent Margin, The Andes—Active Subduction Orogeny. Springer, Berlin, pp. 91–121.
Ranero, C.R., et al., 2008. The hydrogeological system of erosional convergent margins and its influence on tectonics and interplate seismogenesis. Geochem. Geophys. Geosyst. 9 (1–18), Q03S04, http://dx.doi.org/10.1029/2007GC001679.
Ryan, H., von Huene, R., Scholl, D., Kirby, S., 2012. Tsunami hazards to US coasts from giant earthquakes in Alaska. Eos Trans. AGU 93 (19), 185, http://dx.doi.org/10.1029/2012EO190001.
Saffer, D., Tobin, H., 2011. Hydrogeology and mechanics of subduction zone forearcs: fluid flow and pore pressure. Annu. Rev. Earth Planet. Sci. 39, 157–186.
Satake, K., 1994. Mechanism of the 1992 Nicaragua tsunami earthquake. Geophys. Res. Lett. 21, 2519–2522.
Sato, M., Ishikawa, T., Ujihara, N., Yoshida, S., Fujita, M., Mochizuki, M., Asada, A., 2011. Displacement above the hypocenter of the 2011 Tohoku-Oki earthquake. Science 332, 1395, http://dx.doi.org/10.1126/science.1207401.
Solomon, E.A., et al., 2009. Long-term hydrogeochemical records in the oceanic basement and forearc prism at the Costa Rica subduction zone. Earth Planet. Sci. Lett. 282, 240–251.
Suyehiro, K., Nishizawa, A., 1994. Crustal structure and seismicity beneath the forearc off northeastern Japan. J. Geophys. Res. 99, 22331–22347, http://dx.doi.org/10.1029/94JB01337.
Tanioka, Y., Satake, K., 1996. Tsunami generation by horizontal displacement of ocean bottom. Geophys. Res. Lett. 23, 861–864.
Tsuji, T., Ito, Y., Kido, M., Osada, Y., Fujimoto, H., Ashi, J., Kinoshita, M., Matsuoka, T., 2011. Potential tsunamigenic faults of the 2011 off the Pacific coast of Tohoku Earthquake. Earth Planets Space 63, 831–834.
Tsuru, T., Park, J.-O., Miura, S., Kodaira, S., Kido, Y., Hayashi, T., 2002. Along-arc structural variation of the plate boundary at the Japan Trench margin: implication of interplate coupling. J. Geophys. Res. 107, 2357, http://dx.doi.org/10.1029/2001JB001664.
von Huene, R., Klaeschen, D., Cropp, B., 1994. Tectonic structure across the accretionary and erosional parts of the Japan Trench margin. J. Geophys. Res. 99, 22349–22361.
von Huene, R., Ranero, C.R., Vannucchi, P., 2004. Generic model of subduction erosion. Geology 32, 913–916.
Wang, K., Hu, Y., 2006. Accretionary prisms in subduction earthquake cycles: the theory of dynamic Coulomb wedge. J. Geophys. Res. 111, B06410, http://dx.doi.org/10.1029/2005JB004094.
Yamanaka, Y., Kikuchi, M., 2004. Asperity map along the subduction zone in northeastern Japan inferred from regional seismic data. J. Geophys. Res. 109, B07307, http://dx.doi.org/10.1029/2003JB002683.
Yamano, M., Hamamoto, H., Kawada, Y., Ray, L., 2010. Heat flow distribution in the northern Japan Trench area and temperature anomaly in the upper part of the Pacific plate. Japan Geoscience Union Meeting, SCG086-10.
Yamano, M., Kinoshita, M., Goto, S., 2008. High heat flow anomalies on an old oceanic plate observed seaward of the Japan Trench. Int. J. Earth Sci. 97, 345–352.
Yilmaz, O., 2001. Seismic Data Analysis. Society of Exploration Geophysicists, Tulsa, OK.